



MOX-Report No. 35/2018

**Numerical simulations of the microvascular fluid
balance with a non-linear model of the lymphatic system**

Possenti, L.; Casagrande, G.; Di Gregorio, S.; Zunino, P.;
Costantino, M.L.

MOX, Dipartimento di Matematica
Politecnico di Milano, Via Bonardi 9 - 20133 Milano (Italy)

mox-dmat@polimi.it

<http://mox.polimi.it>

Numerical simulations of the microvascular fluid balance with a non-linear model of the lymphatic system

Luca Possenti^{a,*}, Giustina Casagrande^a, Simone Di Gregorio^{a,b}, Paolo Zunino^b, Maria Laura Costantino^a

^a*LaBS, Chemistry, Material and Chemical Engineering Department "Giulio Natta", Politecnico di Milano, Italy*

^b*MOX, Department of Mathematics, Politecnico di Milano, Italy*

Abstract

Fluid homeostasis is required for life. Processes involved in fluid balance are strongly related to exchanges at the microvascular level. A computational model is adopted to study such phenomena mainly relating to oncology, in particular tumor perfusion and related treatments. As far as we know, none of those models consider a physiological non-linear behavior for the lymphatic system. We develop a computational model that consists of a network of straight cylindrical vessels and an isotropic porous media with a uniformly distributed sink term acting as the lymphatic system. In order to describe the lymphatic flow rate, a non-linear function of the interstitial pressure is defined, based on literature data on the lymphatic system. The proposed model of lymphatic drainage is compared to a linear one, as is typically used in computational models. To evaluate the response of the model, the two are compared with reference to both physiological and pathological conditions. A non-physiological behavior is observed when using the linear models of lymphatic drainage but not when using the proposed non-linear model; in addition, differences in local fluid dynamics are found. This work highlights the key role of lymphatic drainage and its modeling when studying the fluid balance in microcirculation for both to

*Corresponding author

Email address: luca.possenti@polimi.it (Luca Possenti)

physiological and pathological conditions, e.g. uremia.

Keywords: uremia, microvascular environment, lymphatic system, fluid homeostasis, interstitial pressure, finite element model

2010 MSC: 00-01, 99-00

1. Introduction

Phenomena involved in fluid homeostasis are related to fluid balance at the microcirculatory level. In order to study such phenomena, different contributions should be considered to describe capillary-to-tissue interactions, including hydraulic and oncotic pressures, capillary wall permeability, microvascular density, blood properties, extravascular properties and the presence of lymphatic vessels. Indeed, the role of lymphatic system can not be neglected when predicting fluid balance. More precisely, lymphatic draining from the interstitial space must be accounted for [1, 2]. In physiological conditions a net filtration rate (NFR) from vessels to interstitial space must be balanced by the lymphatic system to avoid fluid accumulation, which may lead to edema [3, 4]. This process may be altered in some pathology. In such cases, accumulation of fluids within the body is observed. Processes involved in lymphatics function are not fully understood in either physiological or in pathological conditions. On the other hand, a suction effect of lymphatic system leading to sub atmospheric interstitial fluid pressure has been reported and it is widely accepted [2, 5, 6]. However, two main features can be inferred from the literature and the anatomical data. First, the lymphatic system has two different kind of valves in order to ensure unidirectional net flow along lymphatic vessels: primary and secondary valves [2, 7, 8]. Primary valves are located in the lymphatic capillaries (micro-lymphatic or initial lymphatic), whose wall is composed of a monolayer of lymphatic endothelial cells without a continuous basement membrane [2, 9, 10]. These cells form overlapping flap valves with discontinuous button-like junctions [2, 11]. Secondary valves characterize collecting lymphatics vessels. Their presence is directly related to lymph propulsion [2, 8]. These two types of valves contribute to the

unidirectional net flow within the lymphatic system under physiological conditions [2, 9, 10, 12, 13, 14, 15]. A second important feature of the lymphatic capillaries is their interaction with the connective tissue (or extra-cellular matrix) through fibrillin filaments.[2, 4, 6, 16]. These anchoring filaments prevent lymphatic capillaries from collapsing and act by dilating them in response to interstitial pressure increase, eventually increasing wall permeability [9]; thus the wall conductivity can not be considered constant, namely the relationship between pressure and flow rate is non-linear. This non-linearity is reported in the literature, along with an upper limit of the lymphatic drainage which is found to be 20 larger than in typical physiological conditions [1]. Fluid homeostasis has been deeply studied, particularly in reference to pathological conditions such as renal diseases. In these conditions, catabolites are not correctly eliminated, resulting in accumulation of fluids and catabolites (mainly urea) in the body. Uremia, namely the accumulation of end products of metabolism due to renal failure, has been usually studied by means of compartmental models [17, 18, 19]. In such models the whole system, in this case the human body, is divided into subsystems, namely vascular, interstitial and intracellular compartment. Using this approach, variables are assumed not to be dependent on space coordinates but only on time. Even if the key role of capillaries in the fluid balance has been recognized, to our knowledge, models addressing directly the 3D spatial effects of the capillary network and its interaction with the surrounding environment have not been adopted yet to study alterations in fluid homeostasis consequent to uremic pathology. Such a model would be able to account for alterations related to network morphology allowing a deeper study of microcirculation impairment due to uremia. Microvasculature impairment in uremic patients has been reported by multiple studies both in terms of reduced capillary density and worsening of peripheral flow [20, 21, 22, 23, 24].

Although in other fields, such as oncology [25, 26, 27, 28], cerebral flow [29] and tissue oxygenation [30, 31], microcirculation models are already present in the literature, none of them considered a fully physiologic-like behavior of the lymphatic system. However, Siggers and colleagues [32] proposed a model with a

quasi-linear description of lymphatic drainage to prevent lymph back-flow, thus overcoming one of the aforementioned limitations.

Therefore, the aim of this work is to study fluid homeostasis in the microenvironment with reference to uremia; to this end, understanding the correct modeling approach for the action of the lymphatic system in uremia assumes a key role. The micro-scale description of microcirculation allows us to include mechanistic relationships in the model, an improvement with respect to the phenomenological description typical of compartmental models. For this reason, the proposed model enables a more precise control of parameters. As a consequence, we are able to easily discriminate between physiological and pathological conditions, and to describe lymphatic drainage as a non linear function of interstitial pressure, all while also considering also its spatial distribution.

2. Material and methods

A finite element model of microcirculation interacting with the surrounding interstitium has been implemented using GetFEM++ [33]. Starting from a previous work [34], the model has been improved by introducing a more realistic description of the lymphatic system. Then, the model has been tested and used to analyze the fluid balance of the microvasculature. The proposed model is compared with a typical linear model of lymphatic behavior. Both physiological and pathological (uremic) conditions are considered in the analysis in order to evaluate the models in different working points.

2.1. Model description

Following the approach of [34, 35], the microcirculatory network is modeled as a one dimensional (1D) network, immersed in a 3D portion of an isotropic porous medium representing the interstitium. Therefore, this model combines equations on two different domains, Λ the 1D domain describing the capillary network, and Ω , the 3D domain representing the interstitium. The 3D porous medium is described by means of Darcy's law with a hydraulic conductivity k

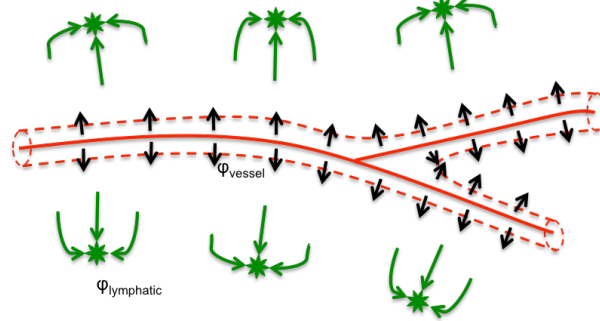


Figure 1: Schematic view of the 3D-1D coupling. 3D vessels geometry (dotted line) and its 1D approximation Λ (continuous line) are shown in red. Fluid exchange in between vessels and interstitium (φ_{vessel}) is indicated by black arrows, and lymphatic drainage from interstitium to lymphatic capillaries ($\varphi_{lymphatics}$) is indicated with green color. Both φ_{vessel} and $\varphi_{lymphatics}$ are computed for each element of the domain Λ and Ω respectively.

and a fluid viscosity μ_t . Blood flow inside the capillaries, considered as cylinders with rigid vascular walls [34], is modeled using Poiseuille's law in terms of vessel radius R and a fluid viscosity μ_v . Lymphatic vessel geometry is usually not included in the simulation of microcirculation [27, 32, 34] due to practical reasons related to the large number of vessels and their dimension. Therefore, the lymphatic drainage is accounted as a distributed sink term in the interstitium continuity equation as a function of tissue properties. A schematic view of the 3D-1D coupling is shown in figure 1.

Using p for hydraulic pressures and u for fluid velocity, the problem to be solved is written as a set of four equations as follows (1):

$$\begin{cases} \frac{\mu_t}{k} \mathbf{u}_t + \nabla p_t = 0 & \text{on } \Omega \\ \nabla \cdot \mathbf{u}_t + \varphi_{lymphatics} - \varphi_{vessels} \delta_\Lambda = 0 & \text{on } \Omega \\ 8 \frac{\mu_v}{R^2} u_v + \frac{\partial p_v}{\partial s} = 0 & \text{on } \Lambda \\ \frac{\partial u_v}{\partial s} + \frac{\varphi_{vessels}}{\pi R^2} = 0 & \text{on } \Lambda \end{cases} \quad (1)$$

where subscripts t and v stand for interstitium and vessels, respectively.

The terms $\varphi_{lymphatics}$ and $\varphi_{vessels} \delta_\Lambda$ in the continuity equation of Ω , model the effects on the interstitium of the lymphatic system and capillary network respectively (figure 1). The latter is described by means of Starling's equation, which considers both the hydraulic and the oncotic pressure (2):

$$\varphi_{vessels} = 2\pi R L_p ((p_v - \bar{p}_t) - \sigma (\pi_v - \pi_t)) \quad (2)$$

where L_p is the hydraulic conductivity of the capillary membrane, σ is the reflection coefficient and π indicates the oncotic pressure. The term \bar{p}_t denotes the average pressure on a cross section of the capillary wall and is computed as described in [34]:

$$\bar{p}_t(s) = \frac{1}{2\pi R} \int_0^{2\pi} p_t(s, \Theta) R d\Theta$$

where s is the *arc length* and Θ is the *angular coordinate*.

2.2. Lymphatic drainage description

Linear models of the net lymphatic drainage are typically defined using a similar approach to the one already used for the capillary vessels [6, 27, 32, 34], based on the Starling's equation (2). Since in our simulations we consider only the vascular geometry and not the geometry of lymphatic vessels, the equation features the term S/V , which is the ratio of exchange surface over the tissue volume. In addition, the high permeability of lymphatic vessels [6, 27, 32, 34] allows us to neglect the oncotic gradient across the membrane obtaining an expression function only of hydraulic pressures (3):

$$\varphi_{lymphatics} = L_{pLF} \frac{S}{V} (p_t - p_l) \quad (3)$$

where subscript l indicates variables referred to the lymphatic system. Knowing the values of $L_{pLF} \frac{S}{V}$ and the physiological reference values of p_t and $\varphi_{lymphatics}$ [36, 37], we have estimated the value of p_l in order to obtain a correct description of the physiological working point.

We propose a new description of the action of the lymphatic system based on a non-linear relation to the interstitial hydraulic pressure. Thus, following the

physiologic description, the net lymphatic flow rate is modeled as a sigmoid function (4), considering a saturation flow rate:

$$\varphi_{lymphatics} = \varphi_{max} - \frac{\varphi_{max} - \varphi_{min}}{1 + \exp\left(\frac{p_t - p_{50}}{slope\ factor}\right)} \quad (4)$$

where φ_{max} and φ_{min} are the maximum and the minimum lymphatic drainage respectively, p_{50} is referred to the interstitial pressure corresponding to $\varphi_{lymphatics} = mean(\varphi_{min}, \varphi_{max})$, and *slope factor* determines the slope of the function. In order to identify parameter values, we refer to Chamney et al. [36] adopting:

- the same increase of pressure necessary to reach the maximum lymphatic drainage from the physiological working point;
- the maximum and minimum values of the lymphatic drainage scaled by the extra-vascular volume [1] to obtain a volumetric term, namely the lymphatic drainage per unit of volume;
- the physiological working point as a couple $(p_t, \varphi_{lymphatics})$, set using the tiny sub-atmospheric interstitial pressure as reported in [37] and the net lymphatic drainage at the physiological working point defined by [36].

A comparison between the proposed non linear models and the linear model of lymphatic drainage as function of interstitial pressure is shown in the figure 2.

2.3. Capillary bed modeling

Different approaches have been used in the literature to describe the capillary bed geometry such as reproducing geometry of a real network [31, 34] or generating artificial network geometry. [29, 30]. Since the focus of this work is the description of the lymphatic drainage, we consider an idealized network geometry with simple boundary conditions. This simplified approach does not replicate a real network geometry but still allows us to investigate the interaction between the network and the surrounding environment. First, let us analyze the basic unit [38] of the geometry (figure 3a). It reproduces the branching of the network including a bifurcation and an anastomosis. Dimensions are set in

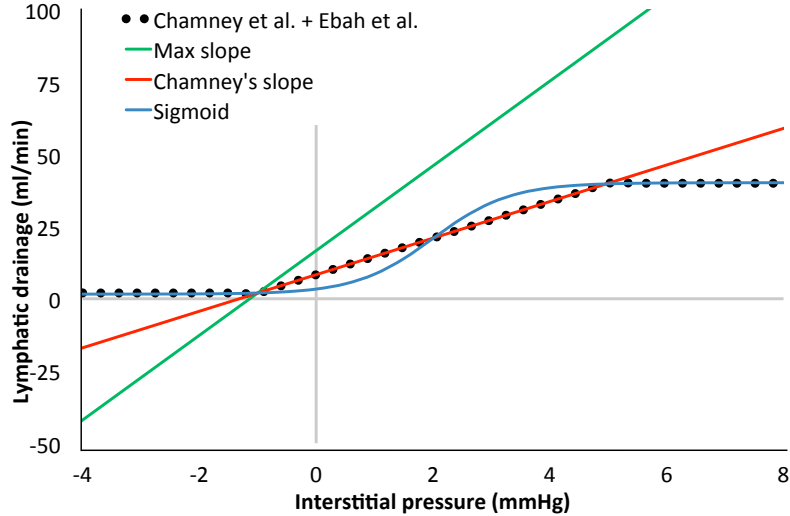


Figure 2: Lymphatic drainage as a function of interstitial hydraulic pressure using different descriptions: (i) Formulation of Chamney et al. [36] adapted to match interstitial pressure at the working point reported by Ebah et al. [37] - dotted black line; (ii) linear formulation (by means of Starling's equation) with lymphatic wall hydraulic conductivity equal to the maximum slope of non-linear function - green line; (iii) linear formulation with lymphatic wall hydraulic conductivity as Chamney et al. [36] - red line; (iv) proposed sigmoid formulation - blue line. Flow rate values are scaled up to the overall extra vascular reference volume equal to 39 l [1].

order to obtain four vessels with the same length, with the two parallel vessels in the middle separated by a $50 \mu m$, as a representative inter-capillary distance [39]. We enforce the hydraulic pressure at both the start and end of this basic unit (from arteriolar to venular side), with higher pressure at the arteriolar side. Considering Starling's equation (2), such pressure conditions mean filtration from the network in the portion characterized by higher pressure, and absorption of fluids near the end. This setup allows us to better discuss our results. We model a vascular network as a repetition of the same basic unit to match the desired capillary density, defined by the $\frac{S}{V}$ ratio. The basic unit is arranged along parallel horizontal planes (as seen in figure 3) along two orthogonal direction to avoid perfect alignment of the network. We keep the higher pressure ends of the units in two adjacent face of the tissue sample, creating

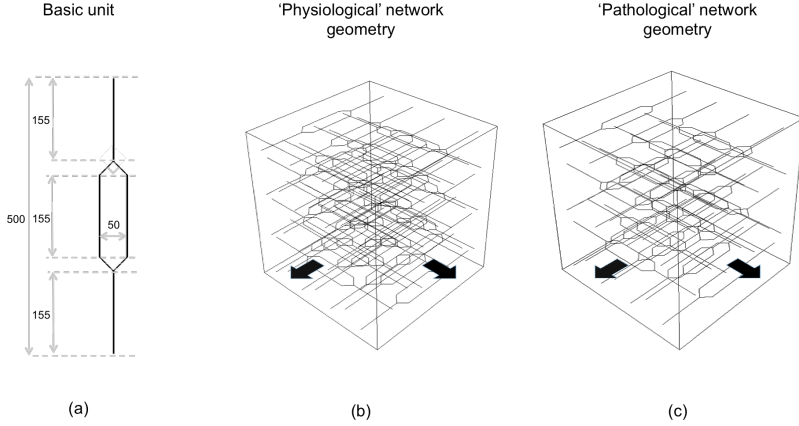


Figure 3: Description of the two different geometries used. They consist of repetition of the basic capillary unit (a) proposed in [38]. The dimensions are in μm . The 3D spatial arrangement of basic units is set to match the desired density, for both physiological (b) and pathological uremic (c) conditions. Arrows indicate the direction of flow in the vessels.

a zone in which we expect mainly filtration and an other in which we expect mainly absorption. To match physiological conditions (figure 3b), we build the network with a $\frac{S}{V}$ ratio equal to $7000 m^{-1}$ [40]. For the pathological case (figure 3c), we note that microvascular impairment has been reported in uremic patients [21, 41]. For example, we refer to [41] to estimate the reduction of capillary density due to uremia. Then, we apply the same reduction (-30%) to the reference physiological condition value obtaining $\frac{S}{V} = 4900 m^{-1}$.

2.4. Numerical methods

The system of equations (1) for the physical variables *vessel fluid velocity* u_v , *vessel hydraulic pressure* p_v , *interstitial fluid velocity* \mathbf{u}_t and *interstitial hydraulic pressure* p_t has been approximated by means of the finite element method. Details about the discretization process of the problem can be found in [34]. The non-linearity due to the proposed lymphatic description is solved using the *fixed-point method*. As a result, the value of $\varphi_{lymphatics}$ is computed considering the hydraulic pressure values of the previous iteration, using a under

relaxation process, if necessary. The stopping criterion for the iterative method is:

$$\begin{aligned} & \frac{\|u_v^k - u_v^{k-1}\|}{\|u_v^{k-1}\|} + \frac{\|p_v^k - p_v^{k-1}\|}{\|p_v^{k-1}\|} + \\ & \frac{\|u_t^k - u_t^{k-1}\|}{\|u_t^{k-1}\|} + \frac{\|p_t^k - p_t^{k-1}\|}{\|p_t^{k-1}\|} < \epsilon \end{aligned} \quad (5)$$

with ϵ equal to 10^{-5} . The spatial grid is tested and selected in order to obtain mesh independent results, resulting in a total number of elements approximately equal to 10^4 .

2.5. Simulations

Numerical simulations were run to investigate the three formulations for the lymphatic drainage. Results obtained using the two linear formulations, based on (3), are analyzed and compared to those obtained with the proposed non-linear formulation (4). All the results of the simulations are evaluated in terms of three variables:

- interstitial fluid pressure (p_t), expressed in *mmHg*;
- lymphatic drainage ($\varphi_{lymphatics}$), expressed in percentage of the maximum admissible value reported in the literature [1, 36];
- vessel to tissue NFR of fluids, expressed in *ml/min*; NFR results are scaled up such that they represent the whole extra-vascular volume in the body [1].

These three variables are presented both in terms of spatial distribution and average values. The average values are computed as an integral mean over the domain considered. These models are tested for both physiological and pathological conditions, with uremia as the modeled pathology; all the cases considered are summarized in Table 1 and explained below.

Comparative evaluation of lymphatic drainage formulations in physiological conditions. As a first step, we analyze the contribution of the lymphatic system under physiological conditions. We define the following cases:

Table 1: Summary of the cases analyzed.

Lymphatic drainage description	Physiological conditions	Pathological conditions (<i>Uremia</i>)
<i>Maximum slope (linear)</i>	CASE A	CASE D
<i>Mean slope (linear)</i>	CASE B	CASE E
Non-linear	CASE C	CASE F

- CASE A: physiological conditions with a linear lymphatic drainage formulation (3) using the maximum slope of the non-linear function (green line in figure 2);
- CASE B: physiological conditions with a linear lymphatic drainage formulation (3) considering the slope defined by Chamney et al. [36] (red line in figure 2);
- CASE C: physiological conditions with the proposed non-linear lymphatic drainage formulation (4) - (blue line in figure 2).

Comparative evaluation of lymphatic drainage formulations in pathological conditions. We compare the three aforementioned formulations also in uremic conditions. In order to model uremia, as shown in Table 2, we have considered the following alterations with respect to the physiological conditions: lower (i) discharge hematocrit, and thus blood viscosity, (ii) capillary wall reflection coefficient, (iii) oncotic pressure gradient (iv) capillary density, and (v) a greater capillary wall hydraulic conductivity. Pathological changes of the lymphatic system and its reaction to pathological conditions need further study to be fully understood [5]. Since no data was found in the literature about changes in lymphatic system between healthy subjects and uremic patients, the aforementioned models are kept without modifications. Therefore, we define:

Table 2: Values of parameter used in the analysis.

Sym- bol	Parameter	Physiologi- cal	Ref.	Pathologi- cal	Ref.
		conditions		conditions	
L	Average capillary length (m)	5×10^{-4}	[42]	5×10^{-4}	[42]
R	Average capillary radius (m)	4×10^{-6}	[1]	4×10^{-6}	[1]
k	Hydraulic conductivity of the tissue (m^2)	10^{-18}	[34, 43]	10^{-18}	[34, 43]
μ_t	Interstitial fluid viscosity ($Pa s$)	1.2×10^{-3}	[43]	1.2×10^{-3}	[43]
H_d	Discharge hematocrit (%)	45	[1]	35	[44, 45]
μ_v	Blood viscosity ($Pa s$)	9.3×10^{-3}	[46]	7.2×10^{-3}	[46]
σ	Capillary wall reflection coefficient (-)	0.95	[3]	0.75	[3, 47]
$\Delta\pi$	Oncotic pressure gradient ($mmHg$)	25	[48]	19	[44, 45]
S/V	Density (m^{-1})	7000	[40]	4900	[40, 41]
L_p	Capillary wall hydraulic conductivity ($m^2 s kg^{-1}$)	10^{-12}	[34]	8.8×10^{-12}	[47]

- CASE D: pathological conditions (uremia) with a linear lymphatic drainage formulation (3) considering the maximum slope of the non-linear function;
- CASE E: pathological conditions (uremia) with a linear lymphatic drainage formulation (3) considering the slope defined by Chamney et al.[36];
- CASE F: pathological conditions (uremia) with the proposed non-linear lymphatic drainage formulation (4).

In addition, a comparison between CASE C and CASE F has been conducted, namely a comparison of the physiological versus pathological conditions using the proposed formulation.

Sensitivity analysis. The effect of parameter variation is tested in a series of simulations. Starting from physiological conditions (CASE C), for each simulation only one parameter at a time is set equal to the pathological conditions (CASE F). Results are analyzed in terms of both NFR and mean interstitial pressure, considering their variation with respect to physiological conditions (CASE C).

Parameters and boundary conditions. Parameters values, reported in the Table 2, were chosen from literature which considered physiological data and studies reporting their change due to the uremic pathology. Unfortunately, quantitative information related to human subjects are not available for all the parameters, due to the difficulty of the measurements: in case of missing information in the literature, variations evaluated in animal studies are considered and compared with human admissible ranges. For example, Harper and colleagues [47] reported a reduction of the reflection coefficient under the admissible range defined by Levick [3]. For this parameter, the lower allowable value is chosen for the analysis. Two different kinds of boundary conditions are considered for the network and the tissue. For the network, we enforce pressure values, precisely 32 mmHg and 15 mmHg at the arteriolar and the venular side of the capillary network respectively [48]. Homogeneous Neumann conditions are considered for the tissue in order to simulate the equilibrium condition, in which no volume is accumulated within the tissue and no net flow rate is leaving the domain. Thus, if we consider \mathbf{n} the normal vector to $\partial\Omega$, the condition is:

$$\mathbf{u}_t \cdot \mathbf{n} = 0 \quad \text{on } \partial\Omega.$$

3. Results

3.1. Comparison of lymphatic modeling approaches in physiological conditions

The different lymphatic drainage formulations are compared in a portion of tissue under physiological conditions (CASE A, B and C). Results in terms of both net lymphatic drainage and interstitial pressure within the domain Ω are shown in figure 4. We visualize with *black color* portions of the domain Ω

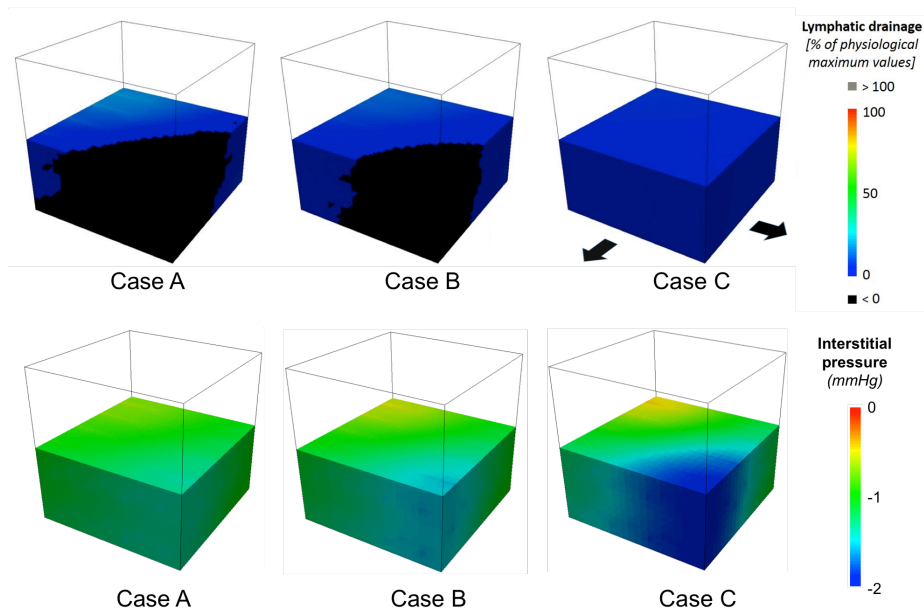


Figure 4: Lymphatic drainage (top) and interstitial fluid pressure (bottom) for physiological conditions considering the three different formulations. Negative lymphatic drainage, that is lymphatic non-physiological behavior, is marked in black. Direction of flow within the vascular network is the same for all the cases shown, and it is indicated by the arrows in the top right case.

characterized by a negative net lymphatic drainage. In such areas, lymphatic net flow is directed from lymphatic capillaries to the tissue. This behavior is seen in both the cases of *linear* model (CASE A and B) but not in the *non linear* model. The resulting interstitial pressure is slightly sub-atmospheric in all the three cases, with values close to -1 mmHg . Lymphatic drainage and interstitial pressure are similar for CASE A and CASE B and different in CASE C. This affinity can be addressed by considering both the mean values (table 3) and spatial distribution (figure 4).

3.2. Comparison of lymphatic modeling approaches in pathological conditions

We compare the different lymphatic drainage formulations also for the case of pathological conditions, namely uremic conditions. As done for physiological

Table 3: Averaged results for both physiological and pathological conditions. Physiological conditions in the upper part of the table (CASE A, CASE B and CASE C), and pathological conditions at the bottom (CASE D, CASE E and CASE F). Net filtration rate (NFR) is scaled to indicate the value for the whole extra-vascular volume in the body [1]. Percentage variations are taken with respect to simulation with the proposed non-linear formulation (CASE C and CASE F).

Physiological	CASE A	CASE B	CASE C
p_t ($mmHg$)	-1.02	-1.04	-1.17
	+13 %	+11 %	-
NFR (ml/min)	1.64	1.69	1.96
	-16 %	-14 %	-
Pathological	CASE D	CASE E	CASE F
p_t ($mmHg$)	3.53	5.58	5.91
	-40 %	-6 %	-
NFR (ml/min)	68.3	43.7	39.6
	+72 %	+10 %	-

conditions, net lymphatic drainage and interstitial pressure are shown in figure 5. In pathological conditions, no lymphatic net back-flow from lymphatic capillaries to tissue is reported. On the other hand, we mark with *grey color* portion of the domain Ω where the net flow rate from tissue to lymphatic capillaries exceeds the maximum admissible value [1, 36]. This behavior is reported for both the *linear* cases (CASE D and E) but not the *non linear* model. On the other hand, CASE E and F show similar results for the mean value of interstitial pressure (table 3). In addition, a gradient of interstitial pressure is seen in all the three cases along the horizontal direction (relative to the orientation of the plots shown in figure 5). This gradient is related to the pressure gradient within the network. Blood is flowing within the capillary network from higher to a

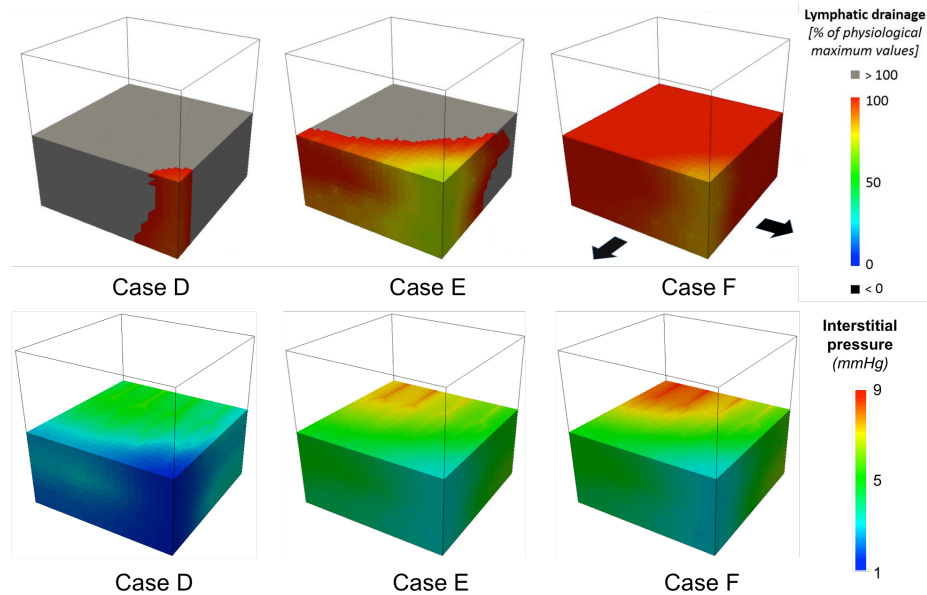


Figure 5: Lymphatic drainage (top) and interstitial fluid pressure (bottom) under pathological conditions is considered for the three different formulation. Excessive drainage, that is lymphatic non-physiological behavior, was marked in grey. Direction of flow within the vascular network is the same for all the cases shown, and it is indicated by the arrows in the top right case.

lower pressure, along the directions indicated by the black arrows in figure 5. Thus, high interstitial pressure and high vascular pressure are located in the same area.

3.3. Sensitivity analysis

We report variations of both averaged interstitial fluid pressure and net filtration rate in figure 6. Since parameters were changed one at a time, the reported variations indicate the contribution of each variable to the overall variation caused by pathological conditions (CASE F, shown in the last column if the figure). This overall effect is not equal to the sum of the single variations, highlighting interactions between parameters. In addition, since $\Delta\pi$ and σ are the most impactful parameters, oncotic pressure difference between blood and interstitium is confirmed as one of the main determinants of the fluid balance

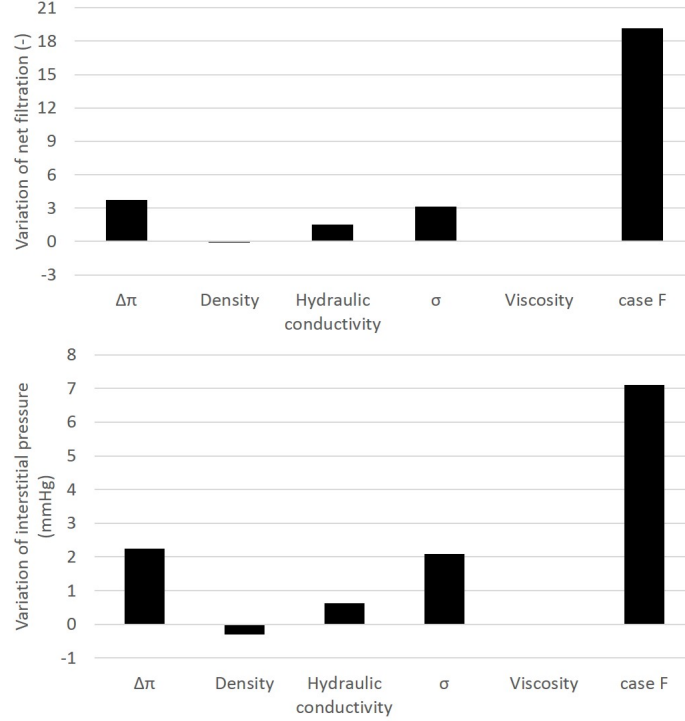


Figure 6: Variation of averaged interstitial fluid pressure (top) and net filtration rate (bottom) produced by the alteration of each parameter with respect to physiological conditions (CASE C). Variations of pressure are computed as $p_{t, i-variation} - p_{t, CASE C}$ (mmHg), whereas for the net filtration rate is calculated as $\frac{\varphi_{vessels, i-variation} - \varphi_{vessels, CASE C}}{\varphi_{vessels, CASE C}}$ (dimensionless).

in the microcirculation. Higher interstitial pressure and intensification of net filtration rate from blood capillaries are found when varying $\Delta\pi$, σ and L_p . On the contrary, a variation of density slightly reduces interstitial pressure. A variation of viscosity, caused by a variation of hematocrit, produces a negligible variation in both output variables considered.

4. Discussion

The results allow us to highlight the key role of lymphatic drainage modeling when describing fluid homeostasis at the microvascular scale. First, we compare

the model performance in both conditions considered and then we analyze how the local phenomena are affected by the modeling approach. Finally, a comparison with the data available in the literature is reported, along with a description of the computational requirements and the study limitations.

4.1. Comparison of lymphatic modeling approaches

In figure 4 we observe that when using the linear modeling approach, the lymphatic system tries to keep interstitial pressure as close as possible to p_l , even if a back-flow is required. Comparing CASE A and B, we conclude that a higher $L_{p,LF}$, namely the hydraulic conductivity of the lymphatic capillary wall, produces larger back-flow zones. Specifically, a higher $L_{p,LF}$ allows for an emphasized action of the lymphatic system (local maximum drainage CASE A: 19%, CASE B: 13%), resulting in a lower variation of interstitial pressure. By considering a *non linear* function, back-flow is prevented in CASE C. Interestingly, this case yields different results with respect to the two above mentioned cases, both in terms of interstitial pressure and NFR with averaged differences bigger than 10%.

Under pathological conditions (CASE D, E and F), since the mean pressure is in between 3.5 mmHg and 5.9 mmHg (table 3), the working point is located in the right part of the figure 2. In these cases, the lymphatic system drains fluid in the whole domain Ω for all the three formulations. On the other hand, we highlight with *grey color* portions of the domain characterized by a net lymphatic flow rate greater than the expected 20-fold increase with respect to physiological conditions [1, 36]. Again, this phenomenon is reported only in the two cases of the *linear model*. As described for physiological conditions, a greater $L_{p,LF}$ generates a stronger lymphatic response and a lower variation of interstitial pressure from the value of p_l (figure 5, CASE D vs E). Surprisingly, similarities in the interstitial pressure are found when analyzing CASE E and F when considering mean values (table 3). This phenomenon can be explained by considering how close the two curves are in figure 2 when hydraulic pressure is equal to 5.5 mmHg .

As a general observation, *linear* models can be used as approximation of a *non linear* phenomenon in precise working conditions. We remark that such an approximation can not be easily applied to 3D models like the one we proposed. Since the value of interstitial pressure is not known *a priori*, the right conditions for the linearization can not be identified (figure 2). Moreover, the interstitial pressure is not constant within the domain Ω (figure 4 and 5). Thus, different working conditions are present in the domain at the same time. On the other hand, a *linear* model can be implemented if one considers mean data (red line in figure 2, and CASE B and E). Our results show that big variations are reported in both the conditions considered, leading to an excessive lymphatic drainage and back-flow. For these reasons, a *non linear* modeling approach is necessary to model fluid homeostasis at the microscale.

In addition, thanks to the sensitivity analysis, the effect of each parameter is highlighted along with their interactions. Indeed, the overall effect, namely CASE F, is not equal to the sum of variations caused by each parameter. Therefore, we point out that a comprehensive modeling approach considering all these variables is necessary to study the problem. Results regarding changes in the viscosity, caused by a variation of hematocrit, are worth noting in particular. It had negligible impact on interstitial pressure and net filtration rate. This observation can be explained by the boundary conditions. Since inlet and outlet pressure are set, a decrease of viscosity, and thus of the resistance of the vessels, would not produce a variation of pressure along the vessel but a variation of flow rate. Consequently, under pathological conditions in CASE F, the microvascular flow rate is greater (+ 29%) than in CASE C. Also results in terms of capillary density should be considered with caution. Its effect should be studied using more a complex network model which includes, for example, the analysis of heterogeneity in hematocrit and viscosity [49].

4.2. Importance of the spatial dependence

Even if 3D computational models of microcirculation are already available in the literature, as far as we know, none of them consider the non-linear behavior

of the lymphatic system. We point out that such a modeling approach is effective provided that the model accounts for the spatial dependence of the pressure. Indeed, even if mean values may look similar for interstitial pressure in table 3, the spatial distribution is different as shown in figure 4 and 5. These local differences and effects are not negligible when trying to accurately describe homeostasis within the microenvironment. Moreover, a gradient in interstitial pressure is always observed in the tissue. It is caused by the interaction with the capillary network. Indeed, the gradient of hydraulic pressure observed within the tissue is similar to the one observed inside the vessels, due to the local interaction in between the two.

4.3. Comparison with the literature

The literature about microvasculature and fluid homeostasis referring to both physiological and uremic conditions at such small scales often reports a big accepted range of variation. In order to compare results of our model with the available data, we consider the analyzed variables: interstitial fluid pressure, net filtration rate and lymphatic drainage.

For the first one, in all the three simulations of physiological conditions, values agree with those reported by Ebah and colleagues [37]. They reported for healthy volunteers an interstitial pressure of $-0.9 \pm 1.3 \text{ mmHg}$. In addition, when the pathological conditions are simulated, interstitial fluid pressure is in the range reported in the same work $4.6 \pm 4.2 \text{ mmHg}$. Therefore, comparing physiological to pathological conditions, the increase of interstitial pressure is correctly reproduced by the model. For NFR, the value reported for the entire body is about 2 ml/min [1], which is in agreement with our results, especially when the non-linear relationship is considered (1.96 ml/min). Under uremic conditions, the increase of pressure is also related to greater NFR from the network to the tissue with a 20-fold growth. Since the equilibrium conditions have been enforced, the net lymphatic drainage balances the net filtration in both cases, with an analogous overall 20-fold increase, reaching the maximum allowable as reported in the literature [1, 36]. Considering the lymphatic model,

different values for the wall permeability can be found in the literature, varying from $4.4 \times 10^{-9} \text{ (Pa s)}^{-1}$ [32], or $10^{-7} \text{ (Pa s)}^{-1}$ [27], to $10^{-6} \text{ (Pa s)}^{-1}$ [40]. The order of magnitude of the proposed model, in terms of mean and maximum slope of the non-linear model, is $10^{-8} \text{ (Pa s)}^{-1}$, within the accepted range.

4.4. Computational requirements

Even if the proposed non-linear description results in a more physiological response of the lymphatic system, its main drawback is the computational cost. Indeed, when the linear formulation is considered, the solution can be obtained by solving the system $\mathbb{A} X = F$; conversely, when the non-linear formulation is used, the system of equations $\mathbb{A} X = F(X)$ is solved by means of the fixed-point method. Even if the computational resources required are higher, we highlight that the non-linear formulation is more adequate to describe phenomena involved in the fluid balance in microcirculation both in physiological and pathological conditions. Such formulation matches the two lymphatics features highlighted in the introduction, namely the back-flow prevention and the variable wall conductivity of the lymphatic capillaries with the fluid interstitial pressure.

4.5. Limitations of the study

In this work, the importance of the particular micro-scale lymphatic description chosen is addressed by means of 3D simulation of fluid homeostasis in microvasculature under both physiological and pathological conditions. A first limitation is the lack of a direct experimental validation. Since measurements at small space scale are difficult to perform, experimental parameter identification and an experimental validation is challenging. Moreover, although this computational tool allows us to compare physiological and pathological conditions, the value of some parameters have not been clearly defined yet, especially in the pathological case. Indeed, the variations induced by uremia have been qualitatively described in the literature, but rarely they have been addressed quantitatively at the microvascular level. Some studies successfully identified

general parameters by means of compartmental models [50], but in order to achieve a microscale description, this approach is not enough. Moreover, we did not include the effects of the glycocalyx on filtration as described by the Micheal-Weinbaum model [51, 52, 53]. They explained how the Starling’s law of filtration can be influenced by this structure, eventually reducing the absorption of fluid by the capillary network. The inclusion of this effect is not straightforward for 3D models, but it is an important future improvement needed to properly describe specific tissues within the body. In addition, high variability of parameters regarding the microvasculature and the surrounding environment is expected and reported both intra-subject, considering different peripheral districts [8, 15], and inter-subject. We do not consider such variability since it is not completely understood [16]. Even considering its limitations, results of the models are meaningful and allow us to highlight the needed for a non-linear modeling approach of lymphatic drainage to properly model fluid homeostasis.

5. Conclusion

The proposed non-linear model of lymphatic system is necessary in order to simulate fluid balance by means of numerical simulation for physiological and in particular for pathological conditions. This work justify the use of a sophisticated 3D/1D microscale computational approach for a localized description of microcirculation fluid balance. It will allow us to analyze the role of capillary density variations and different network morphology (e.g.: tortuosity). Future applications of this model include the study of specific peripheral districts in order to better understand microcirculation worsening related to uremia.

Funding

This research did not receive any specific grant from funding agencies in the public, commercial, or not-for-profit sectors.

Declaration of interest.

None.

Acknowledgements

Authors thank J.T. Loessberg-Zahl for carefully revising the manuscript.

References

- [1] J. Hall, Guyton and Hall Textbook of Medical Physiology 13th Edition, 2015.
- [2] J. E. Moore, C. D. Bertram, Lymphatic System Flows, Annual Review of Fluid Mechanics 50 (1) (2018) 459–482. doi:10.1146/annurev-fluid-122316-045259.
- [3] J. R. Levick, Capillary filtration-absorption balance reconsidered in light of dynamic extravascular factors., Experimental physiology 76 (1991) 825–857. doi:10.1113/expphysiol.1991.sp003549.
- [4] M. Al-Kofahi, J. W. Yun, A. Minagar, J. S. Alexander, Anatomy and roles of lymphatics in inflammatory diseases, Clinical and Experimental Neuroimmunology 8 (3) (2017) 199–214. doi:10.1111/cen3.12400.
- [5] S. Jamalian, M. Jafarnejad, S. D. Zawieja, C. D. Bertram, A. A. Gashev, D. C. Zawieja, M. J. Davis, J. E. Moore, Demonstration and Analysis of the Suction Effect for Pumping Lymph from Tissue Beds at Subatmospheric Pressure, Scientific Reports 7 (1) (2017) 12080. doi:10.1038/s41598-017-11599-x.
- [6] M. A. Swartz, The physiology of the lymphatic system, Advanced Drug Delivery Reviews 50 (2001) 3–20.

- [7] J. P. Scallan, S. D. Zawieja, J. A. Castorena-Gonzalez, M. J. Davis, Lymphatic pumping: mechanics, mechanisms and malfunction, *The Journal of Physiology* 594 (20) (2016) 5749–5768. doi:10.1113/JP272088.
- [8] J. W. Breslin, Mechanical Forces and Lymphatic Transport, *Microvasc Res* 0 (813) (2014) 46–54. doi:10.1016/j.mvr.2014.07.013.
- [9] E. Bazigou, J. T. Wilson, J. E. Moore, Primary and secondary lymphatic valve development: Molecular, functional and mechanical insights, *Microvascular Research* 96 (3) (2014) 38–45. arXiv:15334406, doi:10.1016/j.mvr.2014.07.008.
- [10] J. Trzewik, S. K. Mallipattu, M. Gerhard Artmann, D. F. A., S.-S. G. W., Evidence for a second valve system in lymphatics: endothelial microvalves, *The FASEB Journal* 15 (10) (2001) 1711–1717. doi:10.1096/fj.01-0067com.
- [11] P. Baluk, J. Fuxe, H. Hashizume, T. Romano, E. Lashnits, S. Butz, D. Vestweber, M. Corada, C. Molendini, E. Dejana, D. M. McDonald, Functionally specialized junctions between endothelial cells of lymphatic vessels, *The Journal of Experimental Medicine* 204 (10) (2007) 2349–2362. doi:10.1084/jem.20062596.
- [12] P. Galie, R. L. Spilker, A Two-Dimensional Computational Model of Lymph Transport Across Primary Lymphatic Valves, *Journal of Biomechanical Engineering* 131 (11) (2009) 111004. doi:10.1115/1.3212108.
- [13] E. Mendoza, G. W., Schmid-Schonbein, A Model for Mechanics of Primary Lymphatic Valves, *Journal of Biomechanical Engineering* 125 (3) (2003) 407. doi:10.1115/1.1568128.
- [14] P. M. Lynch, F. A. DeLano, G. W. Schmid-Schönbein, The Primary Valves in the Initial Lymphatics during Inflammation, *Lymphatic Research and Biology* 5 (1) (2007) 3–10. doi:10.1089/lrb.2007.5102.

- [15] K. N. Margaris, R. A. Black, Modelling the lymphatic system: challenges and opportunities, *Journal of The Royal Society Interface* 9 (69) (2012) 601–612. doi:10.1098/rsif.2011.0751.
- [16] D. Vittet, Lymphatic collecting vessel maturation and valve morphogenesis, *Microvascular Research* 96 (2014) 31–37. doi:10.1016/j.mvr.2014.07.001.
- [17] A. A. De Los Reyes V, D. H. Fuertinger, F. Kappel, A. Meyring-Wösten, S. Thijssen, P. Kotanko, A physiologically based model of vascular refilling during ultrafiltration in hemodialysis, *Journal of Theoretical Biology* 390 (2016) 146–155. doi:10.1016/j.jtbi.2015.11.012.
- [18] M. Pietribiasi, J. Waniewski, A. Załuska, W. Załuska, B. Lindholm, Modelling transcapillary transport of fluid and proteins in hemodialysis patients, *PLoS ONE* 11 (8) (2016) 1–22. doi:10.1371/journal.pone.0159748.
- [19] G. Casagrande, C. Bianchi, D. Vito, F. Carfagna, C. Minoretti, G. Pontoriero, G. Rombolà, C. Schoenholzer, M. L. Costantino, Patient-specific modeling of multicompartmental fluid and mass exchange during dialysis, *International Journal of Artificial Organs* 39 (5) (2016) 220–227. doi:10.5301/ijao.5000504.
- [20] K. Amann, E. Ritz, Microvascular disease the Cinderella of uraemic heart disease *, *Nephrology, dialysis, transplantation : official publication of the European Dialysis and Transplant Association - European Renal Association* 15 (September 1999) (2000) 1493–1503.
- [21] Y. C. Yeh, A. Chao, C.-Y. Lee, C.-T. Lee, C.-C. Yeh, C.-M. Liu, M.-K. Tsai, An observational study of microcirculation in dialysis patients and kidney transplant recipients, *European Journal of Clinical Investigation* (2017) 1–8doi:10.1111/eci.12784.
- [22] M. El-Nahid, A. El-Ashmaoui, Functional and structural abnormalities of

- the skin microcirculation in hemodialysis patients, *The Egyptian Journal of Internal Medicine* 26 (3) (2014) 116. doi:10.4103/1110-7782.145307.
- [23] A.-J. Meinders, L. Nieuwenhuis, C. Ince, W.-J. Bos, P. W. Elbers, Haemodialysis Impairs the Human Microcirculation Independent from Macrohemodynamic Parameters, *Blood Purification* 40 (1) (2015) 38–44. doi:10.1159/000380902.
- [24] Y. Benhamou, L. Begarin, N. David, N. Cailleux, C. Bessin, H. Lévesque, S. Edet, Detection of microcirculatory impairment by transcutaneous oxymetry monitoring during hemodialysis: An observational study, *BMC Nephrology* 15 (2014). doi:10.1186/1471-2369-15-4.
- [25] M. Welter, H. Rieger, Interstitial Fluid Flow and Drug Delivery in Vascularized Tumors: A Computational Model, *PLoS ONE* 8 (2013). doi:10.1371/journal.pone.0070395.
- [26] L. Cattaneo, P. Zunino, A computational model of drug delivery through microcirculation to compare different tumor treatments, *International Journal for Numerical Methods in Biomedical Engineering* 30 (11) (2014) 1347–1371. arXiv:NIHMS150003, doi:10.1002/cnm.2661.
- [27] M. Sefidgar, M. Soltani, K. Raahemifar, H. Bazmara, Effect of Fluid Friction on Interstitial Fluid Flow Coupled with Blood Flow through Solid Tumor Microvascular Network, *Computational and Mathematical Methods in Medicine* (2015). doi:10.1155/2015/673426.
- [28] M. Nabil, P. Zunino, A computational study of cancer hyperthermia based on vascular magnetic nanoconstructs, *Royal Society Open Science* 3 (2016). doi:10.1098/rsos.160287.
- [29] N. Safaeian, T. David, A computational model of oxygen transport in the cerebrocapillary levels for normal and pathologic brain function, *Journal of Cerebral Blood Flow & Metabolism* 33 (10) (2013) 1633–1641. doi:10.1038/jcbfm.2013.119.

- [30] D. Goldman, A. S. Popel, A computational study of the effect of capillary network anastomoses and tortuosity on oxygen transport, *Journal of Theoretical Biology* 206 (2) (2000) 181–194. doi:10.1006/jtbi.2000.2113.
- [31] I. G. Gould, A. A. Linninger, Hematocrit distribution and tissue oxygenation in large microcirculatory networks, *Microcirculation* 22 (1) (2015) 1–18. doi:10.1111/micc.12156.
- [32] J. H. Siggers, K. Leungchavaphongse, C. H. Ho, R. Repetto, Mathematical model of blood and interstitial flow and lymph production in the liver, *Biomechanics and Modeling in Mechanobiology* 13 (2) (2014) 363–378. doi:10.1007/s10237-013-0516-x.
- [33] Getfem++ v. 5.0.
URL <http://getfem.org/>
- [34] L. Cattaneo, P. Zunino, Computational models for fluid exchange between microcirculation and tissue interstitium, *Networks and Heterogeneous Media* 9 (1) (2014) 135–159. doi:10.3934/nhm.2014.9.135.
- [35] L. Possenti, S. Di Gregorio, F. M. Gerosa, G. Raimondi, G. Casagrande, M. L. Costantino, P. Zunino, A computational model for microcirculation including Fahraeus-Lindqvist effect, plasma skimming and fluid exchange with the tissue interstitium, Tech. rep., (2018).
- [36] P. W. Chamney, C. Johner, C. Aldridge, M. Krämer, N. Valasco, J. E. Tattersall, T. Aukaidey, R. Gordon, R. N. Greenwood, Fluid balance modelling in patients with kidney failure, *Journal of Medical Engineering and Technology* 23 (2) (1999) 45–52. doi:10.1080/030919099294276.
- [37] L. M. Ebah, H. Wiig, I. Dawidowska, C. O’Toole, A. Summers, M. Nikam, A. Jayanti, B. Coupes, P. Brenchley, S. Mitra, Subcutaneous interstitial pressure and volume characteristics in renal impairment associated with edema, *Kidney International* 84 (5) (2013) 980–988. doi:10.1038/ki.2013.208.

- [38] D. A. Rubenstein, W. Yin, M. D. Frame, *Biofluid mechanics : an introduction to fluid mechanics, macrocirculation, and microcirculation*, 2015.
- [39] J. R. Less, T. C. Skalak, E. M. Sevick, R. K. Jain, *Microvascular Architecture in a Mammary Carcinoma : Branching Patterns and Vessel Dimensions* *Microvascular Architecture in a Mammary Carcinoma : Branching Patterns and Vessel Dimensions*¹, *Cancer research* (265) (1991) 265–273.
- [40] L. T. Baxter, R. K. Jain, *Transport of fluid and macromolecules in tumors. II. Role of heterogeneous perfusion and lymphatics*, *Microvascular Research* 40 (2) (1990) 246–263. doi:10.1016/0026-2862(90)90023-K.
- [41] K. Amann, G. Wiest, G. Zimmer, N. Gretz, E. Ritz, G. Mall, *Reduced capillary density in the myocardium of uremic rats—a stereological study.*, *Kidney international* 42 (5) (1992) 1079–1085. doi:10.1038/ki.1992.390.
- [42] B. J. McGuire, T. W. Secomb, *Estimation of capillary density in human skeletal muscle based on maximal oxygen consumption rates*, *American Journal of Physiology-Heart and Circulatory Physiology* 285 (6) (2003) H2382–H2391. doi:10.1152/ajpheart.00559.2003.
- [43] M. A. Swartz, M. E. Fleury, *Interstitial Flow and Its Effects in Soft Tissues*, *Annual Review of Biomedical Engineering* 9 (1) (2007) 229–256. doi:10.1146/annurev.bioeng.9.060906.151850.
- [44] Database from INTERREG IT-CH 2007-2013: DialysisIS (Dialysis therapy between Italy and Switzerland) Project - Grant ID 33570710., www.dialysis-project.eu.
- [45] D. Vito, G. Casagrande, C. Bianchi, M. L. Costantino, *How to extract clinically useful information from large amount of dialysis related stored data*, *Proceedings of the Annual International Conference of the IEEE Engineering in Medicine and Biology Society, EMBS 2015-November* (2015) 6812–6815. doi:10.1109/EMBC.2015.7319958.

- [46] A. R. Pries, T. W. Secomb, T. Gessner, M. B. Sperandio, J. F. Gross, P. Gaehtgens, Resistance to blood flow in microvessels in vivo, *Circulation Research* 75 (5) (1994) 904–915. doi:10.1161/01.RES.75.5.904.
- [47] S. J. Harper, C. R. Tomson, D. O. Bates, Human uremic plasma increases microvascular permeability to water and proteins in vivo, *Kidney International* 61 (4) (2002) 1416–1422. doi:10.1046/j.1523-1755.2002.00252.x.
- [48] Silverthorn, *Human Physiology*, 2010.
- [49] T. W. Secomb, Blood flow in the microcirculation, *Annual Review of Fluid Mechanics* 49 (2017) 443–461. doi:10.1146/annurev-fluid-010816-060302.
- [50] C. Bianchi, E. Lanzarone, G. Casagrande, M. L. Costantino, Identification of Patient-Specific Parameters in a Kinetic Model of Fluid and Mass Transfer During Dialysis, 2017, pp. 139–149. doi:10.1007/978-3-319-54084-9_13.
- [51] C. C. Michel, Starling: The formulation of his hypothesis of microvascular fluid exchange and its significance after 100 years, *Experimental Physiology* 82 (1) (1997) 1–30. doi:10.1113/expphysiol.1997.sp004000.
- [52] R. H. Adamson, J. F. Lenz, X. Zhang, G. N. Adamson, S. Weinbaum, F. E. Curry, Oncotic pressures opposing filtration across non-fenestrated rat microvessels, *Journal of Physiology* 557 (3) (2004) 889–907. doi:10.1113/jphysiol.2003.058255.
- [53] S. Weinbaum, J. M. Tarbell, E. R. Damiano, The Structure and Function of the Endothelial Glycocalyx Layer, *Annual Review of Biomedical Engineering* 9 (1) (2007) 121–167. doi:10.1146/annurev.bioeng.9.060906.151959.

MOX Technical Reports, last issues

Dipartimento di Matematica
Politecnico di Milano, Via Bonardi 9 - 20133 Milano (Italy)

- 33/2018** Pagani, S.; Manzoni, A.; Quarteroni, A.
Numerical approximation of parametrized problems in cardiac electrophysiology by a local reduced basis method
- 34/2018** Laurino, F.; Coclite, A.; Tiozzo, A.; Decuzzi, P.; Zunino, P.;
A multiscale computational approach for the interaction of functionalized nanoparticles with the microvasculature
- 32/2018** Dal Santo, N.; Deparis, S.; Manzoni, A.; Quarteroni, A.
An algebraic least squares reduced basis method for the solution of nonaffinely parametrized Stokes equations
- 31/2018** Quarteroni, A.
The role of statistics in the era of big data: A computational scientist' perspective
- 30/2018** Ieva, F.; Palma, F.; Romo, J.
Bootstrap-based Inference for Dependence in Multivariate Functional Data
- 29/2018** Manzoni, A.; Bonomi, D.; Quarteroni, A.
Reduced order modeling for cardiac electrophysiology and mechanics: new methodologies, challenges & perspectives
- 28/2018** Gerbi, A.; Dede', L.; Quarteroni, A.
Segregated algorithms for the numerical simulation of cardiac electromechanics in the left human ventricle
- 25/2018** Chave, F.; Di Pietro, D.A.; Formaggia, L.
A Hybrid High-Order method for passive transport in fractured porous media
- 27/2018** Antonietti, P.F.; Verani, M.; Vergara, C.; Zonca, S.
Numerical solution of fluid-structure interaction problems by means of a high order Discontinuous Galerkin method on polygonal grids
- 26/2018** Vergara, C.; Zonca, S.
Extended Finite Elements method for fluid-structure interaction with an immersed thick non-linear structure